Unfolding of collapsed polymers in shear flow: Effects of colloid banding structures in confining channels

Hsieh Chen and Alfredo Alexander-Katz

Department of Materials Science and Engineering, Massachusetts Institute of Technology, Cambridge, Massachusetts 02139, USA

(Received 10 August 2013; revised manuscript received 1 March 2014; published 21 March 2014)

Using hydrodynamic simulations, we demonstrate that confined colloidal suspensions can greatly enhance the unfolding of collapsed single polymers in flow. When colloids come in direct contact with the polymers due to the flow, the collapsed chains become flattened or elongated on the surface of the colloids, increasing the probability of forming large chain protrusions that the flow can pull out to unfold the polymers. This phenomenon may be suppressed if the colloid size is commensurate with the confining channels, where the colloids form well-defined banding structures. Here, we analyze the colloid banding structures in detail and their relation to the chain unfolding. We find that for colloid volume fractions up to 30%, the confined colloids form simple cubic (*sc*), hexagonal (*hex*), or a mixture of $sc + hex$ structures. By directly changing the heights of the confining channels, we show that the collapsed polymers unfold the most in the mixed $sc + hex$ structures. The diffuse (not well-defined) bands in the mixed $sc + hex$ structures provide the highest collision probability for the colloids and the polymers, thus enhancing unfolding the most. Without colloidal suspensions, we show that the confining channels alone do not have an observable effect on the unfolding of collapsed polymers. The well-defined colloid bands also suppress the unfolding of noncollapsed polymers. In fact, the average size for noncollapsed chains is even smaller in the well-defined bands than in a channel without any colloids. The appearance of well-defined bands in this case also indicates that lift forces experienced by the polymers in confinement are negligible compared to those exerted by the colloidal band structures. Our results may be important for understanding the dynamics of mixed colloid polymer solutions.

DOI: 10.1103/PhysRevE.89.032602 PACS number(s): 82.35.Lr, 82.70.Dd

I. INTRODUCTION

Understanding the dynamics of single polymers in flow has been an active research topic for decades because of its close relation to both the rheology of polymer solutions [1] and the emerging technology of manipulating single DNAs [2]. More recently, studies on globular proteins (polymers) have also shown that the protein dynamics in flow directly correlates with the protein functions and stabilities [3,4]. For polymers in a good or Θ solvent (which we refer to as *noncollapsed polymers*) subject to shear flow, the polymers undergo periodic unfolding and refolding cycles as long as the shear rate is faster than the characteristic chain relaxation time [2,5,6]. The averaged polymer extension increases smoothly with increasing shear rates, and there is no well-defined unfolding transition. On the other hand, for polymers in a bad solvent (which we refer to as *collapsed polymers*) subject to shear flow, the polymers show a well-defined unfolding transition at a threshold shear rate [7–9]. To understand the origin of the unfolding of collapsed polymers in flow, a nucleation-based mechanism has been proposed, and the scaling laws derived from this model appear to be in excellent agreement with simulations results [8,9]. The core of this nucleation process involves the concept of thermally excited polymeric protrusions extending from the collapsed chains. The nucleation barrier is overcome when the hydrodynamic drag force acting on a protrusion is larger than the restoring cohesive force, giving rise to the shear rate threshold value.

Recently, we have demonstrated that colloidal suspensions can greatly enhance the unfolding of collapsed polymers [10]. The enhancement comes from colloids colliding with the collapsed chains, increasing the probability of forming large chain protrusions that the flow can pull out to unfold the polymers. Interestingly, we have observed a nonmonotonic enhancement when changing colloid sizes. By analyzing the banding structures of the colloids in confining channels, we have discovered that *commensurability* between the colloids and the channels has a profound effect on the unfolding of polymers. (The colloid sizes are said to be *commensurate* with a channel if the colloids can form well-defined colloid bands within the channel [11].) To the best of our knowledge, there has been no research systematically analyzing the relations of the confined colloid banding structures and polymer unfolding. In this study, we explore such a system providing direct relations between the structure of colloidal bands and the dynamics of polymers within these sheared colloidal dispersions. In particular, we want to understand the effects of commensurability of the colloids and the channels on the unfolding of collapsed and noncollapsed polymers.

Understanding the dynamics of polymers in colloidal suspensions is important since the polymer and colloid mixtures are ubiquitous in our world and found in everyday items such as ink, milk, and paint. However, current research on polymer and colloid mixtures has mainly focused on the microstructures or the phase behavior of the colloids, ignoring the internal degrees of freedom of the polymer chains [12]. We believe that the dynamics of the polymers is as important as that of the colloids, especially in the driven systems.

II. SIMULATION METHODS

In our model system, colloids are simulated as purely repulsive spheres of size r_c and volume fraction ϕ with a no-slip boundary condition at the surface [13]. Single polymers are simulated with $N = 50$ beads of radius a interacting through

 ©2014 American Physical Society

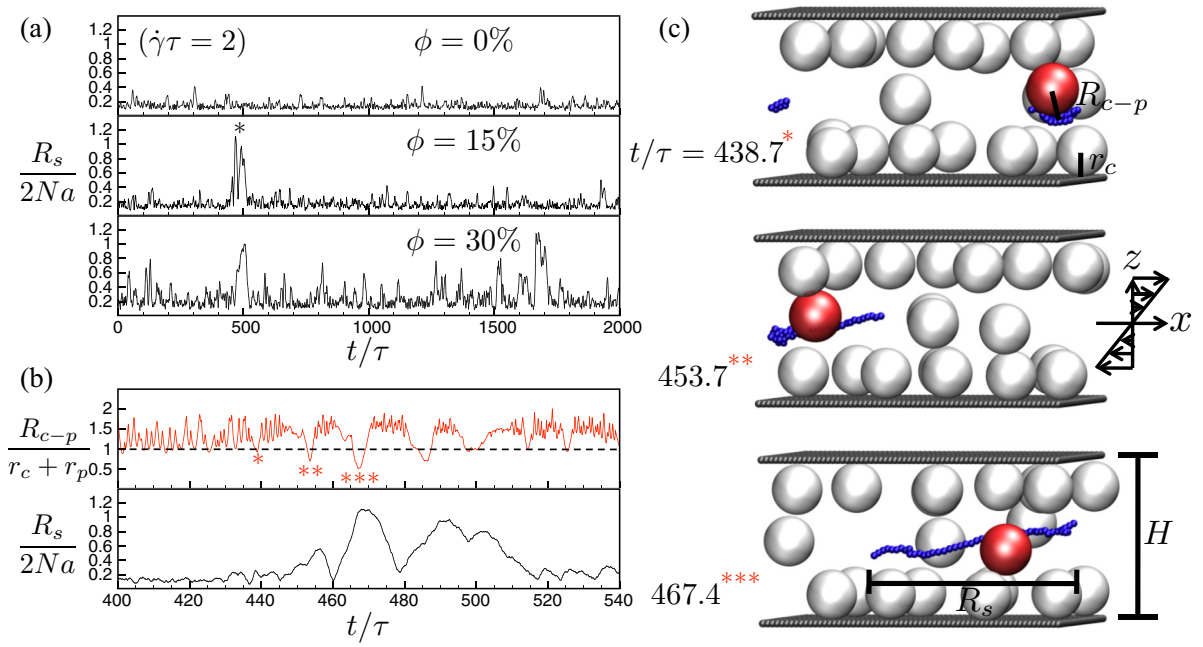

FIG. 1. (Color online) (a) Unfolding sequences for collapsed polymers ($\tilde{\epsilon} = 2.08$) at the same shear rate ($\dot{\gamma}\tau = 2$) but with different colloid volume fractions ($\phi = 0\%$, 15%, and 30%). (b) Time sequences of the nearest colloid distance R_{c-p} (upper sequence; see text for definition) and the polymer extension R_s (lower sequence; see text for definition) for the $\phi = 15\%$ case in (a) from $t/\tau = 400$ to 540, where a well-defined unfolding transition appears. (c) Snapshots of the specific simulation times when a colloid is very close to the polymer. Note that in each snapshot, the polymer is represented by blue beads, the nearest colloid by a red sphere, and other colloids by white spheres.

the intrinsic potential $U = U_s + U_{LJ}$. The first term accounts for the connectivity of the chain,

$$U_s = \frac{\kappa}{2} k_B T \Sigma_{i=1}^{N-1} (r_{i+1,i} - 2a)^2, \tag{1}$$

where $r_{i+1,i}$ is the distance between adjacent beads along the chain. The spring constant is taken to be $\kappa = 800/a^2$, which ensures the average bond length is not larger than 10% of the equilibrium bond length for all the shear rates considered. The second term is a Lennard-Jones (LJ) potential:

$$U_{LJ} = \tilde{\epsilon} k_B T \Sigma_{ij} [(2a/r_{i,j})^{12} - 2(2a/r_{i,j})^6], \tag{2}$$

where $\tilde{\epsilon}$ determines the depth of the potential, and $r_{i,j}$ is the distance between the ith and the jth bead. In this work, we use $\tilde{\epsilon} = 0.41$ for noncollapsed polymers and $\tilde{\epsilon} = 2.08$ for collapsed chains. Every other interaction (i.e., polymer-colloid, colloid-colloid, polymer-wall, and colloid-wall) in the system is purely repulsive, and we use a stiff Hookean interaction that is only present if the distance between two particles is less than the sum of their radii.

The simulation box is bounded in the z direction by no-slip walls separated by a distance H, and periodic boundaries are used in the other two directions. The implicit fluid inside the simulation box is simulated on a three-dimensional grid by the fluctuating lattice-Boltzmann (LB) equation [14], which accounts quantitatively for the dissipative and fluctuating hydrodynamic interactions. For simplicity, we set the grid spacing Δx and the LB time step Δt equal to unity. Other parameters for the fluid are the density $\rho = 1$, the kinematic viscosity $\nu = 1/6$, and the temperature $k_B T = 10^{-4}$. The polymer beads couple to the fluid in a dissipative manner [15]; in LB units, the effective radius of the polymer beads is $a = 0.5$, and the characteristic monomer diffusion time is $\tau = 6\pi\eta a^3/k_B T \cong 4 \times 10^3$, where $\eta = \nu\rho$ is the dynamic viscosity. Detailed descriptions of the simulation methods for the polymers and the colloids can be found in Ref. [16].

III. RESULTS AND DISCUSSION

A. Collisions from colloidal suspensions

Collapsed polymers in shear flow display two dynamical regimes: for low shear rates the chains remain in a compact state, while above a critical shear rate the polymers undergo sudden and repeated unfolding transitions. Recently, we have demonstrated that colloids can greatly enhance the unfolding of collapsed polymers [10,17]. Figure 1(a) presents the typical time sequences of the polymer extension $R_s(t)$ of the collapsed polymers at the same shear rate $\dot{\gamma}\tau = 2$, but with different colloid volume fractions. The polymer extension R_s is defined as the projected polymer length along the flow direction and is illustrated in Fig. 1(c). The effect of colloids is obvious since, for $\phi = 0\%$, the chain remains collapsed, while at higher volume fractions the chain starts exhibiting pronounced and repeated unfolding and refolding events.

To analyze the polymer unfolding in detail, in Fig. 1(b) we replot the time sequence of the polymer extension for the $\phi = 15\%$ case from $t/\tau = 400$ to 540, where a well-defined unfolding transition appears [black star in Fig. 1(a)]. In addition, in Fig. 1(b) we also plot the time sequence of the nearest colloid distance $R_{c-p}(t)$. The nearest colloid distance R_{c-p} is defined as the distance from the polymer center of mass to the center of the nearest colloid. [See Fig. 1(c) for an illustration.] As can be appreciated by examining Fig. 1(b), colloids continuously collide with the polymer. The collisions

occur whenever the normalized distance $\frac{R_{c-p}}{r_c+r_p} \approx 1$, where r_c is the radius of the colloids, and r_p the average radius of the polymer globule. The most important collision for polymer unfolding occurs at $t/\tau = 438.7$ [single red star in Fig. 1(b)], where a colloid compresses the polymer chain into a quasi-two-dimensional pancake globule [the first snapshot in Fig. 1(c)]. Large chain protrusions are formed in this collision event, and the fluid flow is able to unfold the whole chain afterwards. At $t/\tau = 453.7$ and 467.4 [double and triple red stars in Fig. 1(b)], the normalized nearest colloid distance $\frac{R_{c-p}}{r_c+r_p}$ is much less than unity. This behavior occurs because the extended polymer slightly wraps the colloids, and the polymer center of mass resides within the colloid at those moments [second and third snapshots in Fig. 1(c)].

In Fig. 2(a), we show the mean extension $\langle R_s \rangle$ for a collapsed polymer as a function of the dimensionless shear rate $\dot{\gamma}\tau$ for different ϕ's. As can be seen in this plot, the polymer unfolding is clearly enhanced by the colloids and is correlated with the colloid volume fraction. The critical shear rate that is required for the collapsed polymers to unfold decreases from $\dot{\gamma}^*\tau \approx 3$ to 1 when the colloid volume fraction increases from $\phi = 0\%$ to 30%.

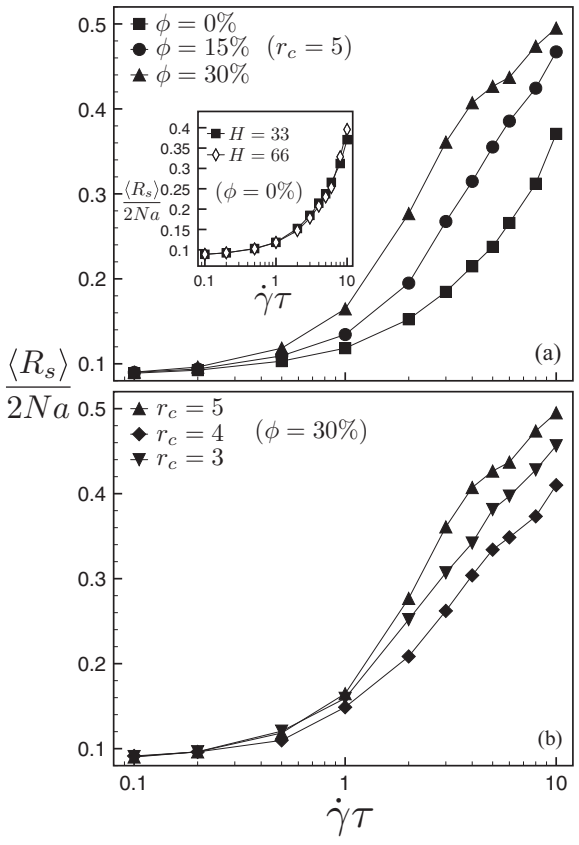

FIG. 2. Rescaled chain extension $\langle R_s \rangle / 2Na$ for collapsed polymers ($\tilde{\epsilon} = 2.08$) as a function of the shear rate $\dot{\gamma}\tau$ for (a) different colloid volume fractions ($\phi = 0\%$, 15%, and 30%) but with a fixed colloid size ($r_c = 5$), and (b) different colloid sizes ($r_c = 3$, 4, and 5) but with a fixed colloid volume fraction ($\phi = 30\%$). Inset in (a): Rescaled chain extension $\langle R_s \rangle / 2Na$ for collapsed polymers ($\tilde{\epsilon} = 2.08$) as a function of the shear rate $\dot{\gamma}\tau$ in empty channels with the channel heights $H = 33$ and 66.

B. Confinement effects

We have shown that confined colloidal suspensions have significant effects on the unfolding of collapsed polymers. However, one might suspect that the confining channels alone also affect the polymer unfolding. The inset in Fig. 2(a) shows the mean extension $\langle R_s \rangle$ for the collapsed polymers as a function of the dimensionless shear rate $\dot{\gamma}\tau$ in empty channels with the channel heights $H = 33$ and 66. Doubling the height from $H = 33$ to 66, we find no significant differences for polymer unfolding. In fact, the mean polymer extension in both the $H = 33$ and $H = 66$ channels is almost identical for all the shear rates considered. In contrast, our previous simulations show that colloids in the channels can alter the critical shear rate for polymer unfolding by up to fivefold [10]. As a result, we conclude that the polymer unfolding is insensitive to the confining channels alone in our simulations.

C. Shear bands with different colloid sizes

In previous sections, we have discussed only the collisions from the single (nearest) colloids with the polymers or the empty confining channels. However, the collective dynamics of the overall colloidal suspensions in the channels also affects the unfolding of polymers drastically. Literature has shown that confined colloidal suspensions exhibit complex ordering transitions under flow, and the transitions highly depend on the commensurability between the colloid sizes and the confining channel dimensions [11]. In a confining channel with a fixed height and colloid volume fraction, we have observed that, for collapsed polymers, the polymer extension $\langle R_s \rangle$ may depend on the colloid sizes r_c nonmonotonically [10]. This interesting result is shown again here in Fig. 2(b), where we have a fixed channel height $H = 33$ and colloid volume fraction $\phi = 30\%$, but with different colloid sizes $r_c = 3$, 4, and 5. When $r_c = 5$ we observe the largest polymer extension, while for $r_c = 4$ we observe the smallest polymer extension with $r_c = 3$ being somewhat in the middle.

To understand the origin of the nonmonotonic polymer extension with the different colloid sizes, we first look at the complex colloid banding structures formed across the confining channels. In particular, we want to realize how the colloid banding structures can affect the collision probability for the colloids and the polymers. In the top panels of Fig. 3, we show the distribution of the polymers (red line) and colloids (black line) as a function of the z position within the channels at a shear rate $\dot{\gamma}\tau = 10$. The green line corresponds to the distribution of the extended polymers and will be discussed later. For the $r_c = 5$ and $r_c = 3$ cases [Figs. 3(a) and 3(c)], only diffuse colloid bands appear in the middle. On the contrary, for the $r_c = 4$ case [Fig. 3(b)], the colloid bands are fully developed. More importantly, the distribution of the polymers is highly regulated by the colloid bands. With the well-defined bands [the $r_c = 4$ case; Fig. 3(b)], the polymers almost always reside between the colloid bands where the collision probability for the colloids and the polymers is the smallest. In contrast, with the more diffuse bands [the

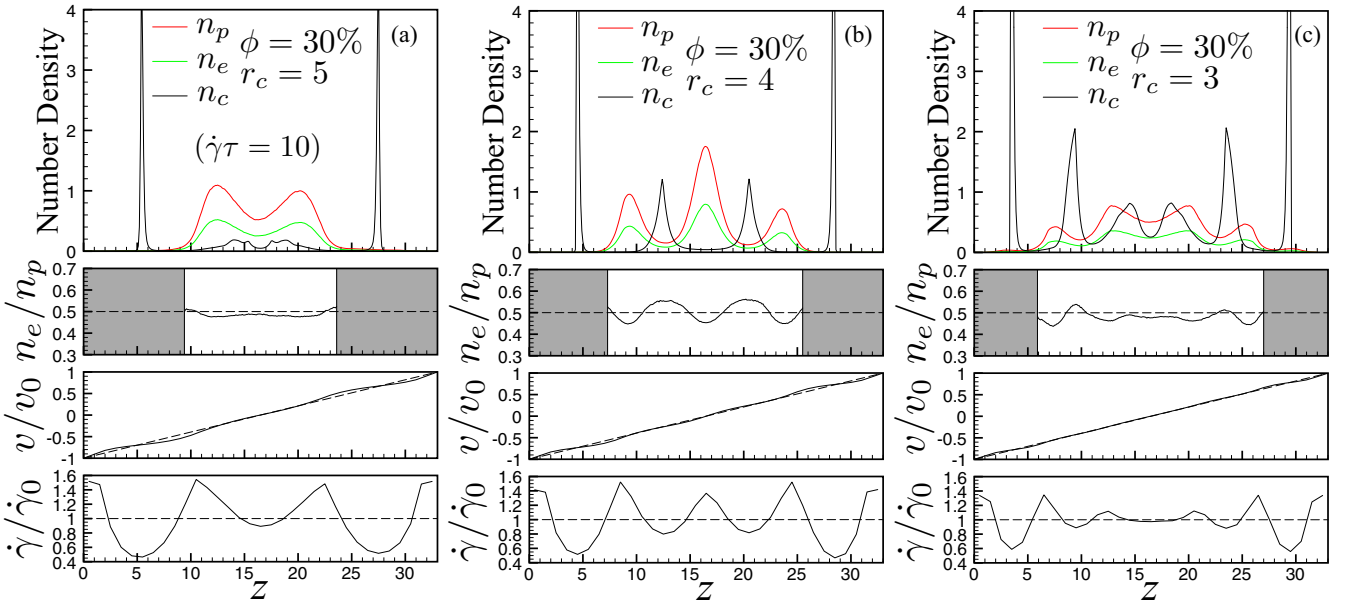

FIG. 3. (Color online) Top panels: Number density of polymers n_p [red (dark gray) line] ($\bar{\epsilon} = 2.08$), extended polymers n_e [green (light gray) line], and colloids n_c (black line) as a function of the z position within the channels at a shear rate $\dot{\gamma} = 10$ and colloid volume fraction $\phi = 30\%$. The extended polymers are defined by the condition $dR_s(t)/dt > 0$. Middle top panels: Number density of the extended polymers divided by the total number density of the polymers. Middle lower panels: Average velocity profile in the x direction. Lower panels: Local rescaled shear rate $\dot{\gamma}/\dot{\gamma}_0$, where $\dot{\gamma}_0$ is the imposed shear rate in the system. The different parts correspond to (a) $r_c = 5$, (b) $r_c = 4$, and (c) $r_c = 3$. Note that the data in the gray areas are removed because the polymer density in those regions is negligible.

$r_c = 3$ and 5 cases; Figs. 3(a) and 3(c)], the polymers are more likely to reside in the colloid bands where the collision probability for the colloids and the polymers is higher. The ratios of the distribution of the extended polymers n_e (green line; see the figure legend for the definition) and the distribution of the polymers in all conditions n_p (red line) are shown in the middle top panels of Fig. 3. This ratio (n_e/n_p) shows the relative probability for the polymers to extend in the channel. As can be more clearly seen in the $r_c = 4$ and $r_c = 3$ cases [Figs. 3(b) and 3(c)], the polymer unfolding is largely enhanced in the colloid bands (where the collision probability for the colloids and the polymers is high), and is suppressed between the bands (where the collision probability for the colloids and the polymers is low). Middle lower and lower panels in Fig. 3 show the velocity profile and the local shear rate in the channel. Although between the shear bands the local shear rate can increase up to 1.5 times higher than the imposed shear rate, the polymer unfolding is not enhanced there. The fact that the polymers unfold more in the colloid bands (where the local shear rate is lower) and unfold less between the bands (where the local shear rate is higher) strengthens our finding that the colloid collision is the main reason for enhancement.

Whether the colloids form the well-defined bands in the channels can be examined by the characteristic gap width η [11]. For a hexagonal packing, the characteristic gap width is defined as

$$\eta_{\text{hex}} = \frac{H - 2r_c}{\sqrt{3}r_c} + 1. \tag{3}$$

On the other hand, for a single cubic packing, the characteristic gap width is simply the channel height divided by the diameter of the colloids,

$$\eta_{sc} = \frac{H}{2r_c}. \tag{4}$$

The colloids and the confining channels are commensurate with each other if the characteristic gap width is close to integers. Table I summarizes the characteristic gap width for the colloids of sizes $r_c = 3, 4$, and 5 in a channel with $H = 33$. For $r_c = 3$ and 5, there are no preferred structures since neither η_{hex} nor η_{sc} for these colloid sizes is close to integer values. In contrast, for $r_c = 4$, the colloids tend to form the simple cubic structure since, here, $\eta_{sc} = 4.13$ is closer to an integer. Table I predicts that the well-defined bands appear only in the $r_c = 4$ case, and this prediction is coincident with our previous analysis of the colloid banding structures (Fig. 3).

Another interesting effect of the dynamic colloidal structures is to completely modify the lift forces experienced by the polymers in confinement. As can be seen in the case in which one has a commensurate system [Fig. 3(b)], the distribution of the polymer is completely dictated by the colloids. In the absence of the latter, the polymer would simply migrate to the center and exhibit a sharp Gaussian-like distribution, as seen in Fig. 9(d). Note that the shear rates in Fig. 3 are higher than

TABLE I. Characteristic gap width for colloids of different sizes in a channel with height $H = 33$.

r_c	η_{hex}	η_{sc}
3	6.20	5.50
4	4.61	4.13
5	3.66	3.30

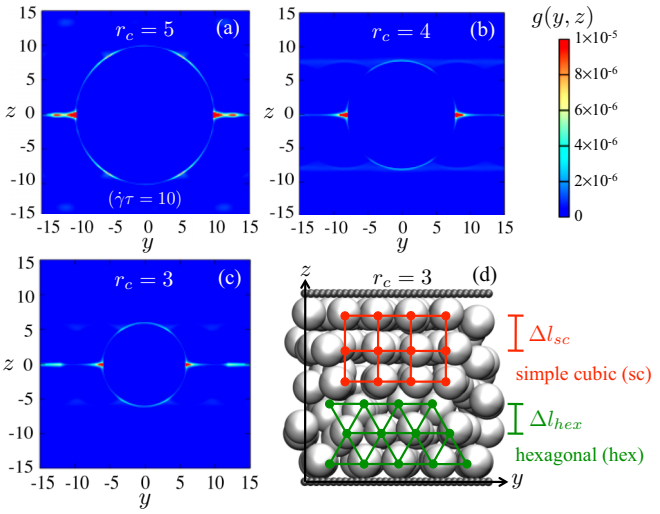

FIG. 4. (Color online) (a) to (c) Radial distribution function in the y-z plane $g(y,z)$ for the colloids with $\phi = 30\%$ in a channel with height $H = 33$. The colloid sizes are (a) $r_c = 5$, (b) $r_c = 4$, and (c) $r_c = 3$. (d) Representative snapshot of the colloids ($r_c = 3$) in the channel. Note that in this special moment, the colloids form the simple cubic structure on the upper part of the channel, and the hexagonal structure on the lower part of the channel.

in Fig. 9, which implies that the lift force is even stronger. Furthermore, the system is already unfolding continuously, which increases the lift force substantially, as L^4, where L is the stretch of the polymer [18]. Compared to the case where no clear bands are formed, we can see that ordering of the colloids induces a strong hydrodynamic force on the polymers. There are of course some steric effects due to excluded volume of the colloids that will expel the polymer from regions of high density, yet the band structure seems to be the most important factor. This issue will be touched upon further in later sections.

To analyze the packing structures predicted in Table I, in Figs. 4(a) to 4(c) we plot the radial distribution function for the colloids in the y-z plane $g(y,z)$. For the $r_c = 4$ case [Fig. 4(b)], $g(y,z)$ shows a clear simple cubic structure. The colloids in different layers distribute directly above or below each other. On the other hand, for the $r_c = 5$ and $r_c = 3$ cases [Figs. 4(a) and 4(c)], $g(y,z)$ shows mixed simple cubic and hexagonal structures. Besides distributing directly above or below each other, the colloids in different layers also pack with mismatches in order to form the hexagonal structures.

In Fig. 4(d), we show a snapshot of the instant colloid distribution for the noncommensurate $r_c = 3$ case. Interestingly, the upper part of the colloids forms the simple cubic structure, while the lower part forms the hexagonal structure. Although instant colloid distribution seems to have well-defined bands, the colloid structures change continuously over time. As shown in Fig. 3(c), for the noncommensurate $r_c = 3$ case, over time the colloids form diffuse structures in the middle of the channel.

D. Shear bands with different channel heights

To study the dynamics of polymers in specific colloidal structures, we directly change the confining channel heights

TABLE II. Characteristic gap width for colloids of size $r_c = 5$ in channels with different heights.

H	η_{hex}	η_{sc}
33	3.66	3.30
36	4.00	3.60
40	4.46	4.00

to match the commensurability of each structure. Table II summarizes the characteristic gap width for colloids of size $r_c = 5$ in three channels with heights $H = 33$, 36, and 40. For $H = 33$, the colloids do not prefer any structures, and $g(y,z)$ analysis [Fig. 4(a)] shows that the colloids form mixed structures. On the other hand, the colloids form the hexagonal (*hex*) structure for $H = 36$, and the simple cubic (*sc*) structure for $H = 40$. Figure 5 shows the average extension for the collapsed polymers as a function of the shear rate in different structures. There are two interesting trends. First, we find that the polymers unfold the most in the mixed *hex* + *sc* structures at all shear rates. Second, comparing the unfolding of the polymers in the specific *hex* or *sc* structures, we find separate dynamical regimes. At the intermediate shear rates, $1 < \dot{\gamma}\tau < 4$, the polymers unfold more in the *hex* structure. However, at higher shear rates $\dot{\gamma}\tau > 4$, the polymer extension is similar in both the *hex* and *sc* structures.

To explain the complex dynamics of the polymers in the different colloid structures and shear rates, we first analyze the colloid banding structures in each condition. Figure 6 shows the colloid and polymer distribution in the different colloid structures (different channel heights) with two shear rates $\dot{\gamma}\tau = 2$ [Figs. 6(a) to 6(c)] and $\dot{\gamma}\tau = 10$ [Figs. 6(d) to 6(f)]. For the mixed *sc* + *hex* structures [$H = 33$; Figs. 6(a) and 6(d)], the colloids form diffuse bands in the middle of the channel, and the polymers intermix with the diffuse colloids to achieve a high collision probability for the colloids and polymers. On the other hand, for the specific *hex* or *sc* structures [$H = 36$ or $H = 40$; Figs. 6(b), 6(c), 6(e), and 6(f)], the colloids form

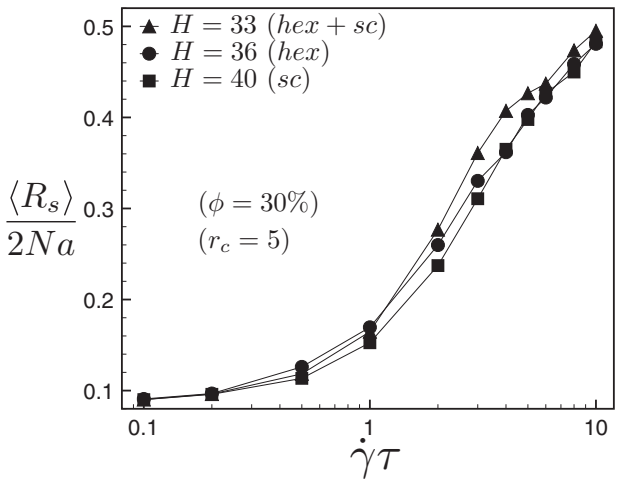

FIG. 5. Chain extension for collapsed polymers ($\tilde{\epsilon} = 2.08$) as a function of the shear rate for the same colloid size $r_c = 5$ and volume fraction $\phi = 30\%$, but with different confining channel heights.

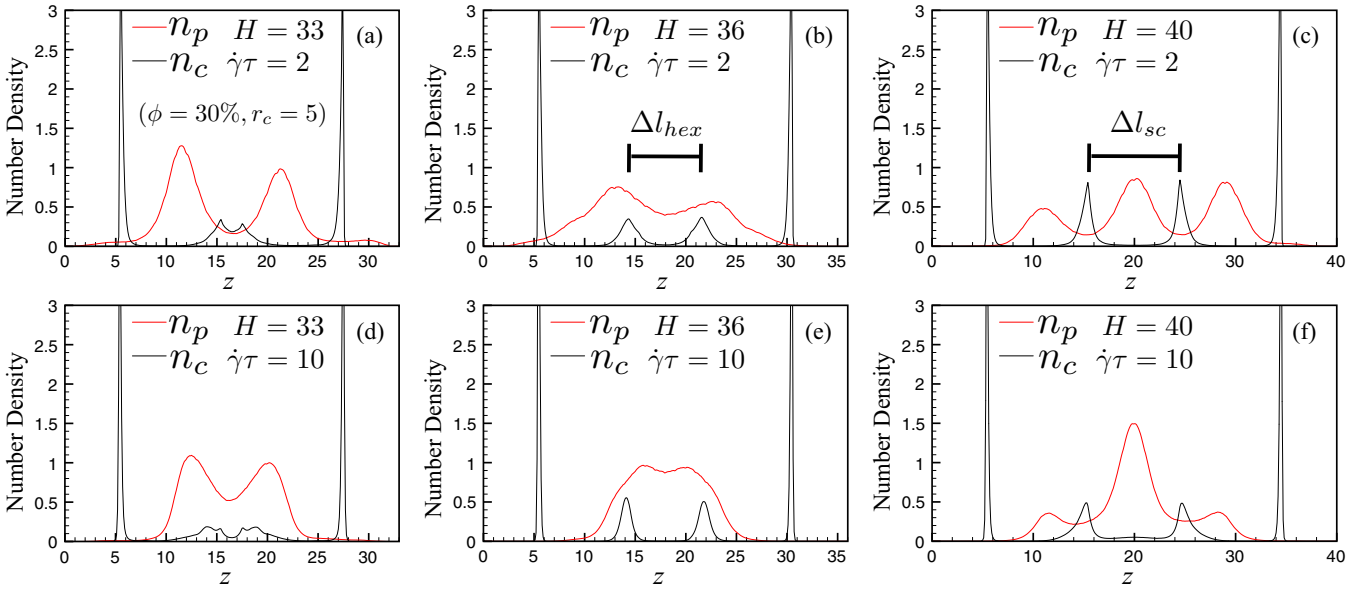

FIG. 6. (Color online) Colloid n_c (black line) and polymer n_p (red line) distribution in the channel with (a) $H = 33$ and $\dot{\gamma}\tau = 2$, (b) $H = 36$ and $\dot{\gamma}\tau = 2$, (c) $H = 40$ and $\dot{\gamma}\tau = 2$, (d) $H = 33$ and $\dot{\gamma}\tau = 10$, (e) $H = 36$ and $\dot{\gamma}\tau = 10$, and (f) $H = 40$ and $\dot{\gamma}\tau = 10$. In all conditions, the colloid size and volume fraction are $r_c = 5$ and $\phi = 30\%$. The collapsed polymers are characterized by $\tilde{\epsilon} = 2.08$.

well-defined bands in the middle of the channels. As can be seen in Figs. 6(b) and 6(c), the distances between bands agree with the packing structures. For the hexagonal packing ($H = 36$),

$$\Delta l_{\text{hex}} = 7.3 \sim 2r_c \sin\left(\frac{\pi}{3}\right) = 8.7. \tag{5}$$

On the other hand, for the simple cubic packing ($H = 40$),

$$\Delta l_{sc} = 9.1 \sim 2r_c = 10. \tag{6}$$

For the simple cubic structure [$H = 40$; Figs. 6(c) and 6(f)], the polymers almost always reside between the colloid bands, as can be seen from the alternating polymer and colloid distribution. One can quickly observe that the polymer and colloid distribution is very similar in both the ($H = 40$ and $r_c = 5$) combination [Figs. 6(c) and 6(f)], and the ($H = 33$ and $r_c = 4$) combination [Fig. 3(b)]. Since the polymers usually reside between the colloid bands where the collision probability for the polymers and colloids is small, the polymers unfold the least in the simple cubic structure. Surprisingly, for the hexagonal structure [$H = 36$; Figs. 6(b) and 6(e)], the distribution of polymers and colloids largely overlaps. This special distribution exists because the hexagonal packing is a much more compact structure, and the empty space between the colloid bands is small. [The relative space between the colloid bands in the *hex* and *sc* structures can be compared in Fig. 4(d).] As a result, the polymers cannot reside between the colloid bands in the *hex* structures. It may seem at first sight that the collision probability for the colloids and polymers is the highest in this distribution. Nevertheless, further analysis (discussed in detail later) shows that the diffuse colloid bands still have the highest collision probability. Comparing the polymer and colloid distribution at low [Figs. 6(a) to 6(c)] and high shear rates [Figs. 6(d) to 6(f)], we find two interesting behaviors. First, the polymers largely concentrate in the middle of the channel at high shear rate. This behavior is due to the hydrodynamic lifting force for polymers and has been thoroughly discussed in the literature [19–21]. It can become a large force [18], and thus deviations from the center can only be accounted for by other strong forces due to the colloids, as we discuss now. Second, when increasing the shear rate, the hexagonal structure is more favorable than the simple cubic

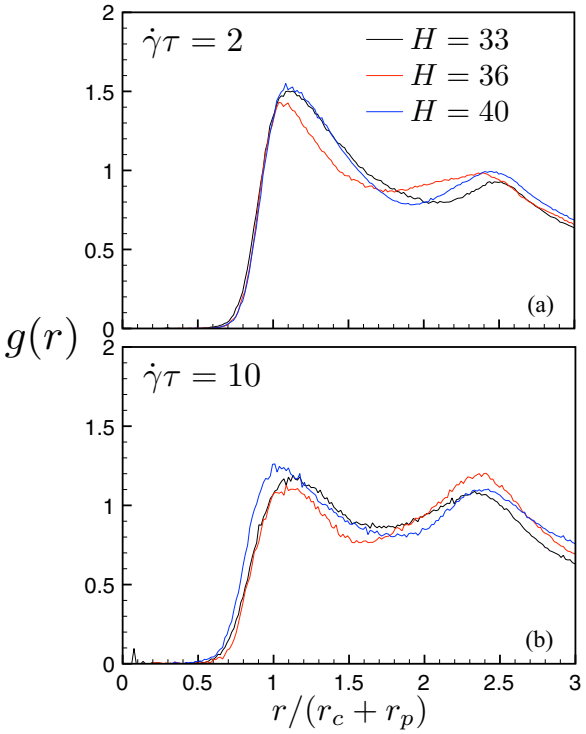

FIG. 7. (Color online) Radial distribution function for colloids to the polymer center of mass with different confining channel heights ($H = 33$, 36, and 40) with shear rates (a) $\dot{\gamma}\tau = 2$ and (b) $\dot{\gamma}\tau = 10$.

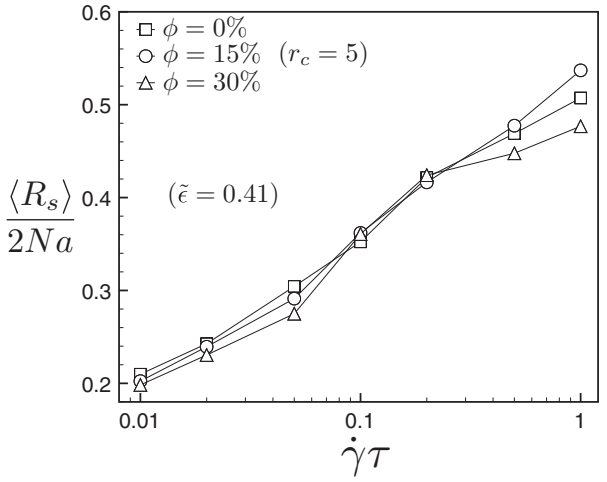

FIG. 8. Average extension for noncollapsed polymers ($\tilde{\epsilon} = 0.41$) as a function of the shear rate with different colloid volume fractions ($\phi = 0\%$, 15%, and 30%).

structure, as can be seen from the increasing *hex* peaks in Figs. 6(b) and 6(e), and the decreasing *sc* peaks in Figs. 6(c) and 6(f). Notice that in Fig. 6(b) the polymer mimics a substitution and does not reside at "interstisial" sites, as for the case of Fig. 6(c).

Analyzing the distribution of the polymers and colloids in the channels is useful to observe the banding structures of the colloids and their relations to the polymers. However, it is sometimes hard to directly extract the collision probability for both components from the banding structures. Thus, we also plot the radial distribution function for the colloids to the polymers $g(r)$ (Fig. 7), where r is now the distance from the colloid centers to the polymer center of mass. As shown, the hexagonal structure ($H = 36$) has the least colloids around the polymers. Nevertheless, it is harder to distinguish between the $H = 33$ and $H = 40$ cases.

E. Noncollapsed polymers in shear bands

The unfolding of noncollapsed polymers starts at lower shear rates and is characterized by a smooth deformation. Instantaneous perturbations by the colloids on the shape of the noncollapsed coils have no obvious effects on the initiation of unfolding. Nevertheless, we do observe interesting behaviors at higher shear rates where the colloids start to form bands. Figure 8 shows the average extension for the noncollapsed polymers as a function of the shear rate $\dot{\gamma}\tau$ for different ϕ's. For all the colloid volume fractions ($\phi = 0\%$, 15%, and 30%), the average extension increases smoothly from $\dot{\gamma}\tau = 0.01$ to 0.2. However, at higher shear rates $\dot{\gamma}\tau > 0.2$, we observe nonmonotonic effects. Compared to a channel without any colloids ($\phi = 0\%$), the average elongation is larger when $\phi = 15\%$ but smaller when $\phi = 30\%$.

Figure 9 shows the distribution of the noncollapsed polymers and colloids in the channels with two shear rates $\dot{\gamma}\tau = 0.1$ and 1, and three colloid volume fractions $\phi = 0\%$, 15%, and 30%. For $\dot{\gamma}\tau < 1$ or $\phi < 30\%$ [Figs. 9(a) to 9(e)], the colloids do not form well-defined bands, and the polymers distribute evenly across the channel and concentrate in the middle. However, at $\dot{\gamma}\tau = 1$ and $\phi = 30\%$ [Fig. 9(f)], the colloids form well-defined bands. Furthermore, the polymer distribution at $\phi = 30\%$ and $\dot{\gamma}\tau = 1$ is different from other cases with lower shear rates or colloid volume fraction. As shown in Fig. 9(f), the polymers distribute much more narrowly between the colloid bands. For the noncollapsed polymers, the smaller average extension within the well-defined bands may result from the smaller polymer coil heights

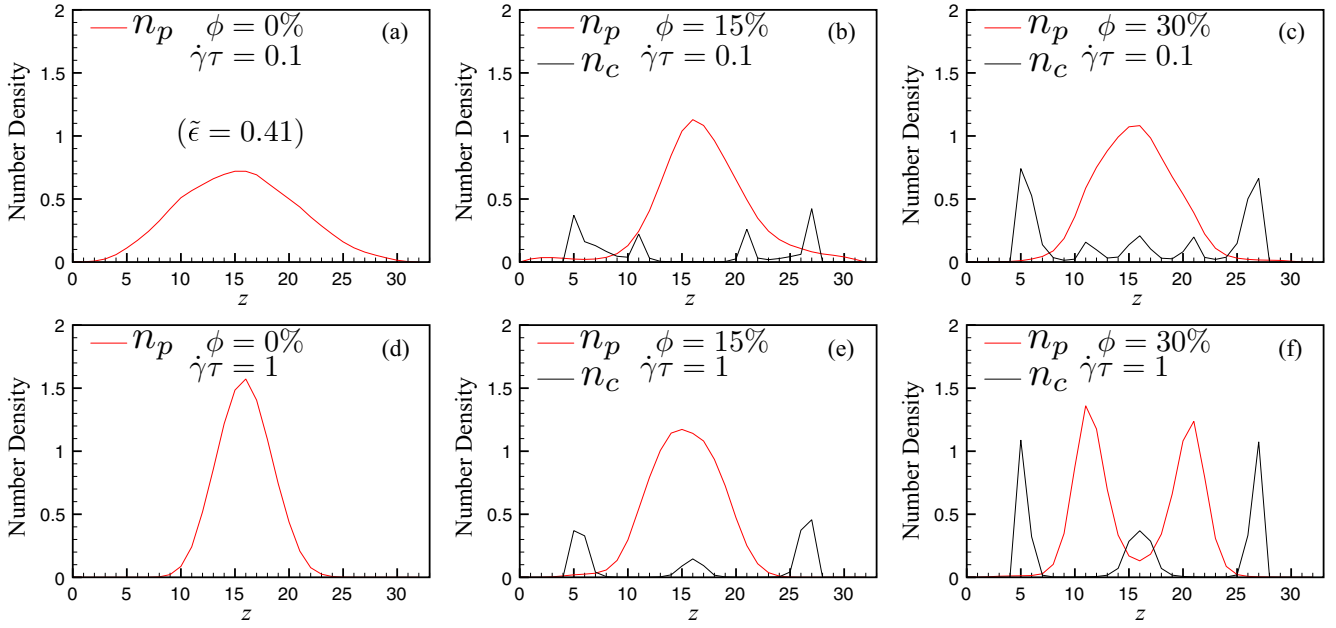

FIG. 9. (Color online) Colloid n_c (black line) and polymer n_p (red line) distribution in the channel with (a) $\phi = 0\%$ and $\dot{\gamma}\tau = 0.1$, (b) $\phi = 15\%$ and $\dot{\gamma}\tau = 0.1$, (c) $\phi = 30\%$ and $\dot{\gamma}\tau = 0.1$, (d) $\phi = 0\%$ and $\dot{\gamma}\tau = 1$, (e) $\phi = 15\%$ and $\dot{\gamma}\tau = 1$, and (f) $\phi = 30\%$ and $\dot{\gamma}\tau = 1$. The noncollapsed polymers are characterized by $\tilde{\epsilon} = 0.41$.

within those bands. (The coil height is defined as the projected height of the polymer coil in the z direction.) Previous studies have shown that the unfolding of the noncollapsed chains is suppressed if the polymers are unable to sample the whole conformation of large coil heights when in confinement [22].

IV. CONCLUSIONS

Confined colloidal suspensions can greatly enhance the unfolding of collapsed polymers in flow. In this paper, we show that the enhancement is mainly due to the collisions from the colloids with the collapsed chains, and the confining channels alone do not have an observable effect on the polymer unfolding. For colloid volume fractions up to 30%, the confined colloids form simple cubic, hexagonal, or a mixture of both structures, depending on the commensurability of the colloid sizes and the channel heights. By changing the colloid sizes or the channel heights, we show that the collapsed polymers unfold the most in the mixed structures because the diffuse colloid bands in these structures provide the highest collision probability for the colloids and the polymers. Lastly, we show that the well-defined colloid bands also suppress the unfolding of noncollapsed polymers. The suppression is due to the redistribution of the noncollapsed polymers within the well-defined bands, where the noncollapsed chains tend to have smaller coil heights. The dynamics of polymers is thus completely controlled by the band structure of the colloids. Further studies in this direction are needed to provide a unified picture on the effects of bands and surfaces on the stability and dynamics of polymer chains.

ACKNOWLEDGMENTS

The authors acknowledge kind support from NSF CAREER Award No. 1054671 and from the DuPont Fellowship. We also want to thank Mike Stopa for his invaluable help with GPU computing and for giving us access to the Orgoglio NNIN/C cluster supported by the FAS Research Computing Group at Harvard University.

[1] R. G. Larson, J. Rheol. **49**, 1 (2005).
[2] D. E. Smith, H. P. Babcock, and S. Chu, Science **283**, 1724 (1999).
[3] S. W. Schneider, S. Nuschele, A. Wixforth, C. Gorzelanny, A. Alexander-Katz, R. R. Netz, and M. F. Schneider, Proc. Natl. Acad. Sci. USA **104**, 7899 (2007).
[4] J. Jaspe and S. J. Hagen, Biophys. J. **91**, 3415 (2006).
[5] P. G. de Gennes, J. Chem. Phys. **60**, 5030 (1974).
[6] P. S. Doyle, B. Ladoux, and J.-L. Viovy, Phys. Rev. Lett. **84**, 4769 (2000).
[7] A. Buguin and F. Brochard-Wyart, Macromolecules **29**, 4937 (1996).
[8] A. Alexander-Katz, M. F. Schneider, S. W. Schneider, A. Wixforth, and R. R. Netz, Phys. Rev. Lett. **97**, 138101 (2006).
[9] A. Alexander-Katz and R. R. Netz, Macromolecules **41**, 3363 (2008).
[10] H. Chen and A. Alexander-Katz, Phys. Rev. Lett. **107**, 128301 (2011).
[11] K. Yeo and M. R. Maxey, Phys. Rev. E **81**, 051502 (2010).
[12] R. Tuinier, J. Rieger, and C. G. De Kruif, Adv. Colloid Interface Sci. **103**, 1 (2003).
[13] C. K. Aidun, Y. Lu, and E.-J. Ding, J. Fluid Mech. **373**, 287 (1998).
[14] B. Dünweg, U. D. Schiller, and A. J. C. Ladd, Phys. Rev. E **76**, 036704 (2007).
[15] P. Ahlrichs and B. Duenweg, J. Chem. Phys. **111**, 8225 (1999).
[16] B. Dünweg and A. J. C. Ladd, Adv. Polym. Sci. **221**, 89 (2009).
[17] H. Chen, M. A. Fallah, V. Huck, J. I. Angerer, A. J. Reininger, S. W. Schneider, M. F. Schneider, and A. Alexander-Katz, Nat. Commun. **4**, 1333 (2013).
[18] C. E. Sing and A. Alexander-Katz, Europhys. Lett. **95**, 48001 (2011).
[19] R. M. Jendrejack, E. T. Dimalanta, D. C. Schwartz, M. D. Graham, and J. J. de Pablo, Phys. Rev. Lett. **91**, 038102 (2003).
[20] R. M. Jendrejack, D. C. Schwartz, J. J. de Pablo, and M. D. Graham, J. Chem. Phys. **120**, 2513 (2004).
[21] R. Kekre, J. E. Butler, and A. J. C. Ladd, Phys. Rev. E **82**, 011802 (2010).
[22] M. Chopra and R. G. Larson, J. Rheol. **46**, 831 (2002).